Silver modified SBA-15 for Iodine entrapment

Micheal P Moloney, Nicolas Massoni, Hans-Conrad Zur Loye, Shani Egodawatte, Agnes Grandjean

Silver modified SBA-15 for Iodine entrapment

Mícheál P. Moloney, ☨¥ Nicolas Massoni, ¥ Shani Egodawatte, ‡ Hans-Conrad zur Loye, δ ‡ Agnès Grandjean δ ☨

☨ CEA, DEN, DE2D, SEAD, Univ. Montpellier, Laboratory of Supercritical and Decontamination Processes, , F-30207 Bagnols-sur-Cèze, France.

¥ CEA, DEN, DE2D, SEVT, Univ. Montpellier, Research Laboratory for the development of conditioning matrices, F-30207 Bagnols-sur-Cèze, France.

δCenter for Hierarchical Waste Form Materials, Columbia, South Carolina 29208, United States.

‡ Department of Chemistry and Biochemistry, University of South Carolina, Columbia, South Carolina 29208, United States

KEYWORDS Solvent free, SBA-15, Silver nanoparticles, Iodine Extraction

ABSTRACT: A green solvent-free approach was used to produce grey colored $Ag/AgNO_3$ functionalized SBA-15. This easy to handle powder was then used to extract molecular Iodine from cyclohexane by simple addition and filtration. The resulting yellow powder was examined by UV-Vis, FT-IR, XRD, TGA and SEM/TEM. It was found that nanosized AgI particles were now present on/in the porous silica support. Despite numerous washing steps with a range of solvents (ranging from cyclohexane to water) no leaching was observed. The sorbent proved highly efficient extracting 0.46 moles of I_2 for every mole of silver, almost 1:1 Ag:I. Finally, TGA demonstrated an increased melting point for AgI indicating a degree of protection from the silica support. This is important when considering transformation into the final waste form.

Although produced in relatively small quantities by the nuclear industry, the extraction and storage of radioactive iodine is important due to its biological sensitivity and long half-life (10^7 years).[1,2] Separately, the upswing in shale gas production has added new interest to this topic as shale gas produced water can have high iodide concentrations, (54mg/L).[3,4,5,6] Although not radioactive or inherently toxic these iodides can interact with other products during the drinking water treatment processes to create harmful by products.[7] The idea of a silver functionalized supports for iodine extraction is hardly new,[8,9,10] Ag-zeolites are typically used in nuclear industry,[1,11,12,13,14] whereas, as radiation is not a concern, in drinking water management Ag functionalized polymers can be used.[3,15,16] Here we expand on

this work and simplify it by removing the need for solvents or stabilising ligands making this approach greener. Taking a process reported by Tang et al. porous SBA-15 and $AgNO_3$ are mixed, crushed and heated together.[17] This simple mixing approach can be easily transposed to other mesoporous support than SBA15. This allows the $AgNO_3$ to decompose and for nanosized metallic Ag^0 particles to be formed in and on the silica structure. This material can then be placed directly into an I_2 solution where it extracts iodine at a ratio of 0.45 I_2 to 1 Ag over 30 minutes. This is almost 1:1 (Ag to I) making it quite efficient visa vie silver use. The silica offers a certain degree of thermal protection to the AgI raising its decomposition temperature; this is important in the nuclear industry when considering this and other materials for long term storage.[18] Here, the unfunctionalized SBA-15, the silver modified Ag@SBA-15 and the I_2 modified AgI@SBA-15 were examined by UV-Vis, FT-IR, XRD, TGA, SEM and TEM. AgI@SBA-15 samples were washed with cyclohexane x2, ethanol x2, acetone x2 and finally water x2. No Ag or AgI particles were detected in the washing. Elemental analysis of the functionalized silica's allowed us to determine the total Ag or AgI particle concentrations. Changes in the surface area and porosity of the samples were examined by N_2 adsorption. The I_2 extraction kinetics and capacity was measured indirectly using UV-Vis. Elemental Analysis (EA) of the silver content of Ag@SBA-15 corresponds well to the initial reactant concentration. 50 mg of $AgNO_3$ were added to 500 mg of SBA-15 to create Ag@SBA-15. This results in a calculated Ag content m/m of 5.8 %. EA (20% error) showed a silver content of 6.4% (weight %). FT-IR of all samples (Ag@SBA-15 and AgI@SBA-15) (SI) showed the typical signals associated with SiO_2.[20] Beyond slight shifts in the frequency of the various Si-O-Si stretches little difference was seen between the samples. These shifts may be a result of the heating process used to incorporate silver into the silica pores. A slight additional frequency change is again seen after addition of I_2. However, this is also seen when I_2 was added to unmodified SBA-15 indicating it is independent of AgI formation.

Solid UV-Vis measurements of Ag@SBA-15 and AgI@SBA-15 are shown in **Figure 1**. The presence of nano size Ag in the Ag@SBA-15 samples is confirmed by the presence of silver plasmon bands at 455 nm.[21,22] After the addition of I_2 the Ag peak is replaced by a strong well-structured e peak at 424 nm.[23,24,25] The position, strength and shape of the peak(s) indicates that monodisperse AgI nanocrystals has now been formed.

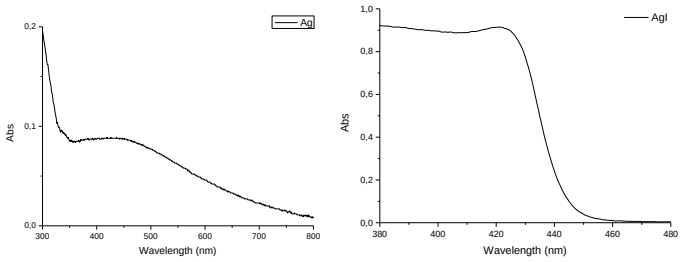

Figure 1: UV-Vis of Ag@SBA-15 (left) and AgI@SBA-15 (right). Ag plasmon band around (left) is completely replaced by AgI exciton peak.

XRD (**Figure 2 and Figure 2 in SI**) confirms the presence of cubic silver (PDF00-001-0503 Fm3m), as well as

the continued presence of silver nitrate (PDF04-011-0004) in Ag@SBA-15 batches. The presence of $AgNO_3$ does not seem to be a problem as after I_2 extraction XRD shows only AgI (a mixture of β, and γ)[26,27] reflections indicating that all detected Ag and $AgNO_3$ has been converted to AgI.

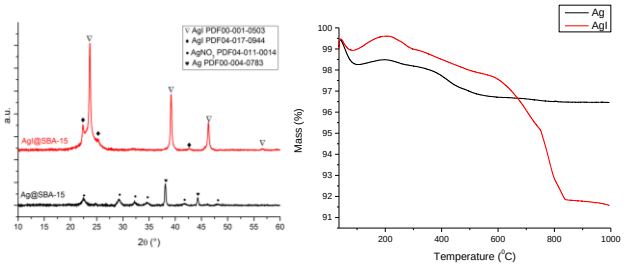

Figure 2: Left; XRD of Ag@SBA-15 (black) and AgI@SBA-15 (red). Note the presence of both Ag and AgNO3 in the Ag@SBA-15 samples. Only AgI is detected after I2 addition. Right; TGA of Ag@SBA-15 (black) and AgI@SBA-15 (red). Mass increase at 200 0C is ascribed to Ag2O formation. However it starts to decompose almost immediately after formation.17,28 Mass loss beginning at 380 0C in the Ag@SBA-15 samples is believed to be AgNO3 decomposition. Mass loss beginning at 600 0C in the AgI@SBA-15 samples is believed to be AgI decomposition.

TGA of the Ag@SBA-15 shows a dehydration step between 30-100 ^{0}C, followed by Ag_2O formation from 100 - 205 ^{0}C. This is in turn followed by its gradual decomposition of Ag_2O. The final mass loss step, beginning at around 380 ^{0}C and finishing at 450 ^{0}C corresponds to the decomposition of $AgNO_3$ (**Figure 2**).[17]

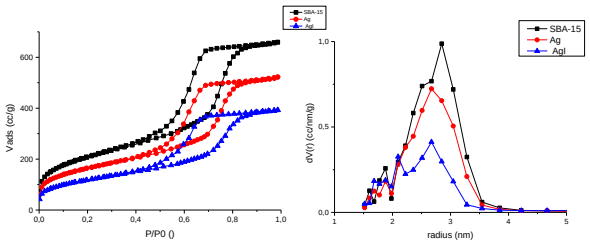

Figure 3: Nitrogen sorption isotherm of SBA-15, (black), Ag@SBA-15, (red) and AgI@SBA-15, (blue).

TGA of the AgI@SBA-15 sample is quite similar to the pure Ag sample at lower temperatures with the dehydration, Ag2O formation/decomposition steps visible No $AgNO_3$ decomposition, step is visible indicating its absence. A large mass step loss slowly begins around 450°C before increasing at 600 ^{0}C with a final steep inflection point at around 700 ^{0}C. These losses are not present in the Ag@SBA-15 TGA curves. The total mass lost (~ 6%) at this temperature corresponds to I_2 content as observed by EA (4.8%). Nitrogen sorption isotherms (**Figure 3** and **Table 1**) showed that the unfunctionalized calcinated SBA-15 has a surface area or 735 m^2/g. This drops to 582 m^2/g batches once functionalized with silver. The surface area is further reduced to 369 m^2/g after I_2 extraction. These reductions in surface area are accompanied by decreases in the pore volume; from 0.98 cm^3/g for SBA-15 to 0.78 (0.495) cm^3/g for the Ag and AgI modified samples respectively.

Table 1: N2 sorption data corresponding to figure 3.

	Surface Area (m^2/g)	Pore Vol. (cm^3/g)	Pore Radius (nm)
SBA-15	729	0.981	2.85
Ag@SBA-15	582	0.784	2.67
AgI@SBA-15	369	0.495	2.66

These decreases indicate that at least some of the silver and consequently the AgI is located inside, or on, the pores of the SBA-15. TEM shows the SBA-15 pores to be around 6 nm in diameter in good agreement with the nitrogen sorption isotherm result. Silver particles (1-3 nm) can be seen freely dispersed inside the pores, however, a large population are either along or on the pore walls. SEM-FEG (Figure 4)shows a dispersion of what EDX (Figure 3 and 4 SI) confirmed was silver throughout the silica. These artefacts are quite large and may represent a macro silver population or large aggregates of individual silver nanoparticles. As UV-Vis (Figure 1) shows only a single silver plasmon band we believe it is the latter. These spots become smaller and more numerous and more disperse after I_2 addition indicating the latter. This again supports the disaggregation of aggregates of individual Ag nanoparticles as AgI is formed. EDX of these bright spots confirms the presence of Ag and I (**Figure 3 and 4 in SI**). The AgI (semiconductor) is now seen as 3 nm white spheres inside the silica pores. This is good agreement with the position and sharpness of the exciton peak seen in Figure 1. Silica pores also appear to have narrower to 3 nm.

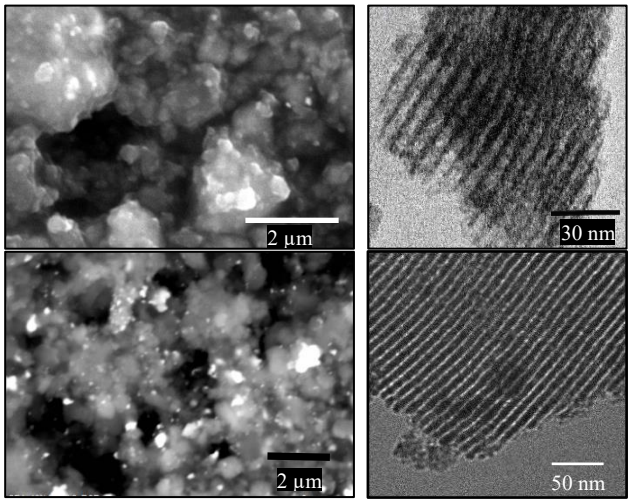

Figure 4: SEM (left) and TEM (right) images Ag@SBA-15 (top) and AgI@SBA-15 (bottom). Silver nanoparticles appear as 3 nm black dots in/on silica pores and pore walls. AgI semiconductor QDs are seen as white dots lined up within the pore network.

Taking these results together, white colored calcinated SBA-15 mesoporous silica was functionalized with $AgNO_3$ nanoparticles through a grinding/ heating method. EA analysis of the resulting grey powder confirmed that no silver had been lost during functionalisation. UV-Vis confirmed the presence of Ag nanoparticles. Ag@SBA-15 showed a silver plasmon band at 455 nm, (**Figure 1**). While XRD confirmed that cubic silver had been formed it also showed that $AgNO_3$ was also still present, (**Figure 2**). This would explain the relatively low concentration of silver nanoparticles as seen in UV-Vis. TGA showed water loss below 100 ^{0}C as well as Ag oxidation at 210 ^{0}C followed by Ag_2O decomposition, all of which is recorded in the literature.[17] A large mass loss for the silver modified samples is also present at around 450 ^{0}C (**Figure 2**). Total weight loss above 600 ^{0}C was 3.6 %. This is in very good

agreement with the total nitrate content 3.67 % as extrapolated from EA. It therefore appears that any free nitrate (liberated from the reduced silver) is also retained, possibly sorbed by the SBA-15 or used to passivate the newly formed silver surfaces. Nitrogen sorbtion isotherms show a decrease in surface area, pore size and pore volume of the SBA-15 after modification with silver nitrate, (**Figure 3/Table 1**). This would seem to suggest that the silver particles are in/on or covering the pores. SEM and TEM confirmed all three, although the degree of aggregation made imaging difficult. Silver particles are visible in the pore spaces with a sizable population clearly visible along the pore walls. The average particle size appears to be around 3 nm, (**Figure 4**). However due to lack of a stabiliser the degree particle aggregation is high. Although the population is almost entirely spherical one or two truncated triangles were seen. SEM shows the presence of large 100-500 nm bright spots on the Ag@SBA-15, (**Figure 4**). EDX confirmed that this was silver. Therefore, silver structures are also present on the outside of the SiO_2. After addition of the grey Ag@SBA-15 powder to an I_2 cyclohexane solution yellow AgI@SBA-15 was formed. This is confirmed by both UV-Vis and XRD. Despite numerous washing steps using initially cyclohexane, followed by ethanol, then acetone and finally water, no leaching was observed. This combined with the highly structured UV-Vis signals (despite the absence of a surface passivating stabiliser) suggests that the AgI is well bound to the silica. That is the AgI surface is being passivated with silanol groups. Also, both UV-Vis and XRD now shows only AgI peaks/reflections respectively. Considering that washing steps resulted in no leaching this would suggest that all Ag^0 particles and $AgNO_3$ has been converted to AgI. While not surprising for the $AgNO_3$ (as it is a classic Ag source for AgI formation), it would seem that instead of forming Ag/AgI core shell particles all Ag particles have been converted to AgI. This is probably the result of the Kirkendall effect, allowing for diffusion of iodine throughout the silver particles, instead of simply forming an AgI shell around an Ag core.[29,30] This makes this material highly efficient for I_2 extraction. SEM of the AgI@SBA-15 shows a dramatic change in the appearance of surface silver artefacts. The large micron sized Ag aggregates have been replaced by smaller (70-300nm) more monodisperse looking nanocrystals. This suggests that the large artefacts seen on the Ag@SBA-15 were not silver microparticles but aggregates of silver nanoparticles or perhaps physiosorbed $AgNO_3$. Either scenario would help explain the high I_2 capacity exhibited by these materials. In the case of $AgNO_3$ it is a matter of chemical conversion. If the silver is present as aggregated Ag^0 nanoparticles then the addition of the strongly nucleophilic iodine to the silver surface would aid in surface charge separation, causing the silver aggregates to disassemble thereby allowing the iodine to access all particles within the aggregate.[31] Nitrogen sorption isotherms showed that the pore volume continued to decrease after I_2 addition indicating that AgI is also formed within the pores. TGA measurements of the AgI@SBA-15 showed an additional mass loss step at 600-820 ^{0}C. While this is assumed to be AgI decomposition the temperature is

relatively high as the literature records the melting point of AgI nanoparticles at 550 ^{0}C.[32] However, according to EA the Iodine content of AgI@SBA-15 is 4.8%. This is in good agreement with these mass loss steps indicating that it is AgI decomposition with the accompanying loss of I_2. This higher melting point indicates again that the AgI is being stabilised by the silica.

I_2 Sorption Kinetics and capacity

The rate of I_2 extraction was measured indirectly using UV-Vis. A known mass of I_2 was dissolved in a fixed volume of cyclohexane giving a violet solution with a strong absorption peak at 522 nm. Its molar extinction coefficient (ε) was calculated and used to determine the amount of I_2 removed from solution after a fixed amount of Ag@SBA-15 was added. As a control the behaviour of unfunctionalized SBA-15 in this I_2 solution was also observed. It was found to sorb a very small amount of I_2 which resulted in the silica having an orange yellow hue. This is probably due to the silanol groups on the SiO_2 hydrolysis the molecular I_2. The silica would later release the iodine yellowing its container walls. This therefore is probably how the AgI is formed in the case of the Ag@SBA-15. The SBA-15 sorbed and then hydrolysed small amounts of I_2 which the Ag then converts to AgI. This process continues until all the silver has been used. Initial extraction is quite fast with 50% of total I_2 sorbed after 1 minute (Figure 5). At this stage I_2 uptake slows considerably with equilibrium been reached after 30 minutes. A Langmuir plot was used to calculate extraction capacity which was found to be 68 mg/g (corresponding to TGA and EA results); 68 mg of I_2 equals 5.4 mmoles of I^-. (Figure 5)

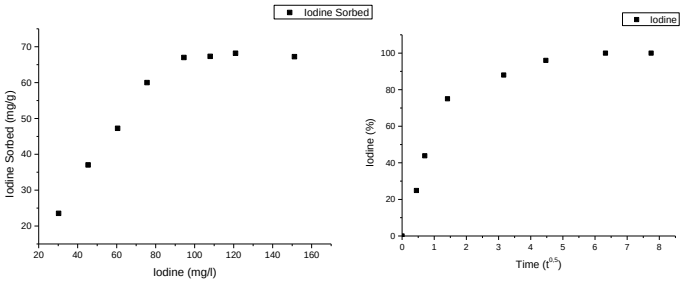

Figure 5: Left kinetics of I2 extraction in minutes onto Ag@SBA-15. Right: Langmuir plot showing the I2 capacity of Ag@SBA-15. Iodine (mg/L) => equilibrium concentration.

As 1g AgI@SBA-15 of contains 5.9 mmoles Ag this puts the actual yield of AgI (where Ag is the limiting factor) at 92.5%. Neither XRD nor UV-Vis detected any remaining Ag after I_2 addition allowing us to conclude that this value is within experimental error of near quantitative efficiency.

In conclusion, silver functionalized porous silica was prepared by a green solvent-free approach. XRD showed that metallic silver was present while UV-Vis and TEM showed that the silver was present as Ag° nanoparticles. While the conversion of the silver precursor did not go to completion, (presence of $AgNO_3$) this did not affect the I_2 extraction. It was found that the conversion of Ag to AgI was almost 100 % indicating perhaps a Kirkendall effect had taken place. This type of effect is well recorded in the literature. Washing with a number of solvents ranging from cyclohexane to water resulted in no AgI leaching indicating that the particles are well bound to the silica. UV-Vis of the

AgI also indicated a well-structured and passivated surface. SEM also suggested a disaggregation effect after I_2 addition. This further influenced us to believe that any large Ag objects seen on the silica were aggregated nanoparticles and not bulk silver. The presence of unstabilised nano sized silver particles presented a large silver surface area which allowed for rapid I_2 extraction with a half-life of 1 minute, and a total conversion with a ratio Ag:I equal to 1:1. Finally, the thermal behaviour of this material with a high stability up to 600°C allows consideration to transform this kind of silica based materials into a final waste form by thermal treatment to close the porosity.

ASSOCIATED CONTENT

Supporting Information. Experimental details, FT-IR scans, XRD diffractogramand EDX spectra are available as Supporting Information should be included, ending with "This material is available free of charge via the Internet at http://pubs.acs.org."

AUTHOR INFORMATION

Corresponding Author

* Agnès Grandjean. E-mail : agnes.grandjean@cea.fr

Author Contributions

The manuscript was written through contributions of all authors. / All authors have given approval to the final version of the manuscript. ‡These authors contributed equally. (match statement to author names with a symbol)

Funding Sources

Research was conducted in part by the Center for Hierarchical Waste Form Materials (CHWM), an Energy Frontier Research Center (EFRC) supported by the U.S. Department of Energy, Office of Basic Energy Sciences, Division of Materials Sciences and Engineering under Award DE-SC0016574. We also thank the EDDEM-CEA project for funding this work.

Notes.

ACKNOWLEDGMENT

Elemental Analysis was carries out by the Laboratoire de métallographie et d'analyse chimique, DEN/MAR/SA2I/DIR, CEA Marcoule, France.

ABBREVIATIONS

REFERENCES

1. Chapman, K. W.; Chupas, P. J.; Nenoff, T. M., Radioactive Iodine Capture in Silver-Containing Mordenites through Nanoscale Silver Iodide Formation. Journal of the American Chemical Society 2010, 132 (26), 8897-8899.
2. Haefner, D. R. T., T. J., Methods of Gas Phase Capture of Iodine from Fuel Reprocessing Off-Gas: A Literature SurVey. Idaho National Laboratory 2007.
3. Li, J.; Wang, M.; Liu, G.; Zhang, L.; He, Y.; Xing, X.; Qian, Z.; Zheng, J.; Xu, C., Enhanced Iodide Removal from Water by Nano-Silver Modified Anion Exchanger. Industrial & Engineering Chemistry Research 2018, 57 (51), 17401-17408.
4. Harkness, J. S.; Dwyer, G. S.; Warner, N. R.; Parker, K. M.; Mitch, W. A.; Vengosh, A., Iodide, Bromide, and Ammonium in Hydraulic Fracturing and Oil and Gas Wastewaters: Environmental Implications. Environmental Science & Technology 2015, 49 (3), 1955-1963.
5. Parker, K. M.; Zeng, T.; Harkness, J.; Vengosh, A.; Mitch, W. A., Enhanced Formation of Disinfection Byproducts in Shale Gas Wastewater-Impacted Drinking Water Supplies. Environmental Science & Technology 2014, 48 (19), 11161-11169.
6. Collins, A. G., CHEMISTRY OF SOME ANADARKO BASIN BRINES CONTAIINING HIGH CONCENTRATIONS OF IODIDE. Chemical Geology 1969, 4 (1-2), 169-187.
7. Hua, G. H.; Reckhow, D. A.; Kim, J., Effect of bromide and iodide ions on the formation and speciation of disinfection byproducts during chlorination. Environmental Science & Technology 2006, 40 (9), 3050-3056.
8. Karkhanei, N.; Sepehrian, H.; Cheraghali, R., Preparation, characterization, and iodide sorption perfor-

mance of silver-loaded mesoporous MCM-41. Desalination and Water Treatment 2015, 56 (11), 3096-3105.

9. Matyas, J.; Canfield, N.; Sulaiman, S.; Zumhoff, M., Silica-based waste form for immobilization of iodine from reprocessing plant off-gas streams. J. Nucl. Mater. 2016, 476, 255-261.

10. Riley, B. J.; Kroll, J. O.; Peterson, J. A.; Matyas, J.; Olszta, M. J.; Li, X. H.; Vienna, J. D., Silver-Loaded Aluminosilicate Aerogels As Iodine Sorbents. ACS Appl. Mater. Interfaces 2017, 9 (38), 32907-32919.

11. Agency, I. A. E., Treatment, conditioning and disposal of iodine-129. 1987.

12. Small, L. J.; Krumhansl, J. L.; Rademacher, D. X.; Nenoff, T. M., Iodine detection in Ag-mordenite based sensors: Charge conduction pathway determinations. Microporous and Mesoporous Materials 2019, 280, 82-87.

13. Liu, Y.; Chen, F.; Wasylishen, R. E.; Xu, Z. H.; Sawada, J.; Kuznicki, S. M., A Study of Silver Species on Silver-Exchanged ETS-10 and Mordenite by XRD, SEM and Solid-State Ag-109, Si-29 and Al-27 NMR Spectroscopy. Journal of Nanoscience and Nanotechnology 2012, 12 (8), 6420-6427.

14. Chibani, S.; Chebbi, M.; Lebegue, S.; Bucko, T.; Badawi, M., A DFT investigation of the adsorption of iodine compounds and water in H-, Na-, Ag-, and Cu- mordenite. Journal of Chemical Physics 2016, 144 (24).

15. El-Gendi, A.; Samhan, F. A.; Ismail, N.; El-Dein, L. A. N., Synergistic role of Ag nanoparticles and Cu nanorods dispersed on graphene on membrane desalination and biofouling. J. Ind. Eng. Chem. 2018, 65, 127-136.

16. Sanchez-Polo, M.; Rivera-Utrilla, J.; Salhi, E.; von Gunten, U., Removal of bromide and iodide anions from drinking water by silver-activated carbon aerogels. Journal of Colloid and Interface Science 2006, 300 (1), 437-441.

17. Tang, Y.; Yang, M.; Dong, W.; Tan, L.; Zhang, X.; Zhao, P.; Peng, C.; Wang, G., Temperature difference effect induced self-assembly method for Ag/SBA-15 nanostructures and their catalytic properties for epoxidation of styrene. Microporous and Mesoporous Materials 2015, 215, 199-205.

18. zur Loye, H. C.; Besmann, T.; Amoroso, J.; Brinkman, K.; Grandjean, A.; Henager, C. H.; Hu, S. Y.; Misture, S. T.; Phillpot, S. R.; Shustova, N. B.; Wang, H.; Koch, R. J.; Morrison, G.; Dolgopollova, E., Hierarchical Materials as Tailored Nuclear Waste Forms: A Perspective. Chemistry of Materials 2018, 30 (14), 4475-4488.

19. Egodawatte, S.; Zhang, E.; Posey, T. J.; Gimblet, G. R.; Foulger, S. H.; zur Loye, H.-C., Synthesis of Scintillating Ce3+-Doped Lu2Si2O7 Nanoparticles Using the Salt-Supported High Temperature (SSHT) Method: Solid State Chemistry at the Nanoscale. ACS Applied Nano Materials 2019, 2 (4), 1857-1865.

20. Zhang, X.; Huang, N.; Wang, G.; Dong, W.; Yang, M.; Luan, Y.; Shi, Z., Synthesis of highly loaded and well dispersed CuO/SBA-15 via an ultrasonic post-grafting method and its application as a catalyst for the direct hydroxylation of benzene to phenol. Microporous and Mesoporous Materials 2013, 177, 47-53.

21. Agnihotri, S.; Mukherji, S.; Mukherji, S., Size-controlled silver nanoparticles synthesized over the range 5–100 nm using the same protocol and their antibacterial efficacy. RSC Advances 2014, 4 (8), 3974-3983.

22. Aherne, D.; Ledwith, D. M.; Gara, M.; Kelly, J. M., Optical properties and growth aspects of silver nanoprisms produced by a highly reproducible and rapid synthesis at room temperature. Adv. Funct. Mater. 2008, 18 (14), 2005-2016.

23. Kobayashi, Y.; Misawa, K.; Takeda, M.; Kobayashi, M.; Satake, M.; Kawazoe, Y.; Ohuchi, N.; Kasuya, A.; Konno, M., Silica-coating of AgI semiconductor nanoparticles. Colloids and Surfaces A: Physicochemical and Engineering Aspects 2004, 251 (1), 197-201.

24. Chebbi, M.; Azambre, B.; Cantrel, L.; Koch, A., A Combined DRIFTS and DR-UV–Vis Spectroscopic In Situ Study on the Trapping of CH3I by Silver-Exchanged Faujasite Zeolite. The Journal of Physical Chemistry C 2016, 120 (33), 18694-18706.

25. Tofanello, A.; Araujo, J. N.; Nantes-Cardoso, I. L.; Ferreira, F. F.; Souza, J. A.; Lim, D.-W.; Kitagawa, H.; Garcia, W., Ultrafast fabrication of thermally stable protein-coated silver iodide nanoparticles for solid-state superionic conductors. Colloids and Surfaces B: Biointerfaces 2019, 176, 47-54.

26. Wang, Y.; Mo, J.; Cai, W.; Yao, L.; Zhang, L., Large-scale synthesis of β-AgI nanocrystals. Materials Letters 2002, 56 (4), 502-506.

27. He, H.; Wang, Y.; Chen, H., Synthesis and room temperature photoluminescence of AgI nanoparticles embedded in silica sol–gel coating. Solid State Ionics 2004, 175 (1), 651-654.

28. Herley, P. J.; Prout, E. G., THE THERMAL DECOMPOSITION OF SILVER OXIDE. Journal of the American Chemical Society 1960, 82 (7), 1540-1543.

29. Yin, Y. D.; Rioux, R. M.; Erdonmez, C. K.; Hughes, S.; Somorjai, G. A.; Alivisatos, A. P., Formation of hollow nanocrystals through the nanoscale Kirkendall Effect. Science 2004, 304 (5671), 711-714.

30. Qin, Z. H.; Sun, H. Y.; Jiang, Z.; Jiao, X. L.; Chen, D. R., Synthesis of metal sulfide nanoboxes based on Kirkendall effect and Pearson hardness. Crystengcomm 2013, 15 (5), 897-902.

31. Mulvaney, P.; Linnert, T.; Henglein, A., SURFACE-CHEMISTRY OF COLLOIDAL SILVER IN AQUEOUS-SOLUTION - OBSERVATIONS ON CHEMISORPTION AND REACTIVITY. J. Phys. Chem. 1991, 95 (20), 7843-7846.

32. Liu, H.-S.; Wang, Y.-H.; Li, C.-C.; Tai, C. Y., Characterization of AgI nanoparticles synthesized in a spinning disk reactor. Chemical Engineering Journal 2012, 183, 466-472.

Insert Table of Contents artwork here